Optimal Allocation of DGs in Radial Distribution Networks Based on Improved Salp Swarm Algorithm

Hongyu Long, Shun Pan, Tingting Xu, Xinyu Liu*, Sheng Xia, Cheng Yao, Hu Lu

Abstract—**In radial distribution networks, the unreasonable use of distributed generators (DGs) will enhance the effects of voltage quality reduction and network loss. Consequently, the optimal allocation of distribution groups (OADG) has far-reaching implications for the economical, secure, and stable operation of radial distribution networks. The purpose of the study on the optimal allocation of distributed generators is to allocate the locations and capacities of DGs scientifically and rationally, enhance voltage quality, and reduce power loss. This paper proposes an enhanced ISC-SSA algorithm with constraint strategy for the OADG problems, which addresses the disadvantages of traditional salp swarm algorithm (SSA), such as low solution accuracy and slow convergence speed, and introduces a sine cosine algorithm (SCA) to optimise the salp swarm followers. To reduce the limitation of only the leader guiding the followers for position updates, a symbiotic strategy with multiple subpopulations is introduced to simulate the sharing of information of the salp swarm population, relying on the decision-maker and the leader to jointly guide the population movement, thereby increasing the global optimization-seeking capability of the algorithm, and the method is implemented in IEEE-33, IEEE-69, and IEEE-119 systems.**

In addition, the paper extends the ISC-SSA algorithm to the MOISC-SSA algorithm to solve in IEEE-33, IEEE-69 test systems the multi-objective OADG problems. Multiple sets of simulation results demonstrate that the proposed method solves radial distribution system problems of varying sizes with greater search precision and greater significance.

Manuscript received January 19, 2023; revised June 6, 2023. This work was supported by the Science and Technology Project of State Grid Chongqing Electric Power Company(5220002000C0: Research on key technologies of electric vehicle charging and replacement based on big data driven and digital twin deduction).

Hongyu Long is a professor-level senior engineer of Chongqing University of Posts and Telecommunications, Chongqing 400065, China (e-mail: longhongyu20@163.com).

Shun Pan is a graduate student of Chongqing University of Posts and Telecommunications, Chongqing 400065, China (e-mail: p_scqupt@163.com).

Tingting Xu is a senior engineer of State Grid Chongqing Electric Power Company Marketing Service Center, Chongqing, 400014, China (e-mail: Xu_tingting_cq@163.com).

Xinyu Liu* is a professor-level senior engineer of State Grid Chongqing Electric Power Company, Chongqing 400014, China (corresponding author to provide phone: +8613996108500; e-mail: liuxinyu_cq@163.com).

Sheng Xia is a professor-level senior engineer of Chongqing Jiangbeizui Water Air Conditioning Co., Ltd., Chongqing, 404100, China (e-mail: xiasheng_cq@163.com).

Cheng Yao is a senior engineer of Chongqing Public Transport Group Bayi Site Management Company, Chongqing 400020, China (e-mail: yaocheng_cq@163.com).

Hu Lu is a professor-level senior engineer of Chongqing Jiangbeizui Water Air Conditioning Co., Ltd., Chongqing, 404100, China (e-mail: luhu_cq@163.com).

Index Terms — **Distributed generators (DGs), Optimal allocation, Sensitivity factor, ISC-SSA algorithm**

I. Introduction

The current distribution network is facing a dramatic increase and diversification of loads, and the distribution network is becoming more complex than ever. The power generated by traditional production methods is becoming more and more difficult to cope with society's requirements for power quality, economy, environmental protection, and reliability of power supply systems in today's rapidly developing social economy [1,2]. With the advancement of technology, distributed generators are gradually being used in distribution systems, allowing the network to be in a reliable and economical state [3].

DGs connected to the distribution network will change the nature of the network from radial to reticulated compared to the main station, which has better flexibility. Due to the low-voltage and high-current characteristics of the distribution network, the losses caused during the transmission and distribution of electricity in the distribution network are the largest in the power system [4]. DGs integrated into the distribution network have been proven to be one of the most economical measures to address network loss [5]. Through this way, power can be digested locally, saving transmission, substation investment, and operation costs, improving voltage distribution, effectively reducing power losses in the grid [6], complementing the large grid power supply, improving peak and valley performance of the grid and increasing power supply reliability.

The integration of DGs into the distribution network is a complex and combinatorial planning problem, which will lead to increased power losses, voltage instability, and poor system reliability if the DGs are installed in an inappropriate location with an improper capacity [7]. The general objective function of the DGs configuration problem is to reduce network loss and improve voltage distribution or reliability improvement, and the literature [8-10] has identified power loss as the main objective for configuring DGs. In addition, considering other optimizable metrics in the network, the literature [11] considers active power loss, voltage distribution, and voltage stability index(VSI) as targets for configuring DGs; The literature [12] uses an improved rainfall optimization algorithm to reduce active power loss and operating costs to enhance voltage quality and VSI on buses 33 and 69.

It is demonstrated that the essence of the OADG problem resides in the consideration of constraints and the

optimisation of high-quality distributed power allocation subject to the satisfaction of constraints. The typical approach to constraints is the penalty function method (PFM), and the literature [13] employs multiple penalty factors to maximise energy purchase cost, energy loss cost, emission penalty cost, demand deviation penalty, operation and maintenance cost, and net present value profit of renewable energy investment in order to achieve economic investment planning for DGs and battery storage systems. The literature [14] considers the minimization of corporate costs as the objective function to solve relay allocation and power distribution problems with the penalty function. The distribution network is a large-scale network, and the failure of OADG problems to accomplish zero constraint violations in the distribution network may result from the use of inappropriate penalty factors. This paper proposes a new constraint policy to assure that the configurations of DGs do not contravene any system constraints, based on the OADG problems.

In addition to the treatment of constraint strategies, numerous heuristic intelligent algorithms have been extensively implemented in OADG problems to Improve the operation performance of the system. Literature [15,16] presents an enhanced algorithm under constraint strategy for determining the optimal configuration of distributed power supplies to minimise active power loss and enhance voltage stability, respectively. The authors in the literature [17,18] improved the convergence speed and search accuracy of the algorithm to reduce losses in the distribution system. The authors of the research [19] contrasted four distinct algorithms to simulate the behaviour of renewable distributed generators based on various penetration levels, employing probabilistic optimal tide techniques to reduce power losses. The authors of the research [20] considered the determined power demand and employed the Symbiotic Search for Organisms (SOS) algorithm to determine the optimal location and capacity of DGs to reduce network losses.

The optimal configurations of DGs can be divided into two parts of the problem; The single-objective problem focusing on minimising the active power loss while the multi-objective problem attempting to take into account more metrics. The conventional treatment for multi-objective problems is to transform each objective into a single objective using a weighted approach. In [21], the Whale Optimisation Algorithm (WOA) was utilised to optimise the configuration and size of distribution static compensators in a radial distribution network with the goals of minimising power losses, enhancing voltage distribution, and boosting network reliability. In [22], the GASBO hybrid algorithm was utilised to reduce line losses and voltage deviation while simultaneously reducing the grid's total emissions. This strategy is appropriate for situations in which the decision maker has a distinct bias towards a particular objective. Many researchers elect to use Pareto optimality to seek for feasible optimal sets of multi-objective OADG problems in order to derive objectively optimal Pareto frontier (PF) allocation schemes. The literature [23] proposes the Pareto frontier differential evolution (PFDE) algorithm for 33-bus and 69-bus systems to increase voltage stability, decrease power losses, and boost network voltage. The authors of [24] propose an improved Raven Roost Optimisation (IRRO) algorithm for determining the optimal distribution of DGs in radical distribution networks in order to increase technical and economic efficiency. Unlike the multi-objective processing method with weighted transformation into a single objective, the Pareto optimal search method can be used to obtain multiple feasible objective composition schemes, allowing decision-makers to choose the outcome based on a variety of options.

In this paper, the constraint priority replaces the traditional penalty function, and the Sine Cosine - Salp Swarm algorithm (ISC-SSA) is proposed for the single-objective problem of OADG in three different sizes of test systems. In addition, this article employs a novel MOISC-SSA algorithm for multi-objective problems, which obtains a more uniform Pareto distribution in 33-bus and 69-bus test systems. The article's structure is as follows. In Section II of this paper, the mathematical models of OADG are introduced. Section III describes the constrained prior strategy, the algorithm, and its enhancement. The results and analysis of the simulation experiments are presented in Section IV. Section V gives the conclusion of this paper.

II. Formulation

The optimal configuration of DGs includes the treatment of objective functions and constraints. This section describes the two objective functions and lists the constraints that are satisfied in the OADG problem.

A. Objective Functions

Fig. 1 abstractly represents a single-wire structured power distribution system with *n* nodes.

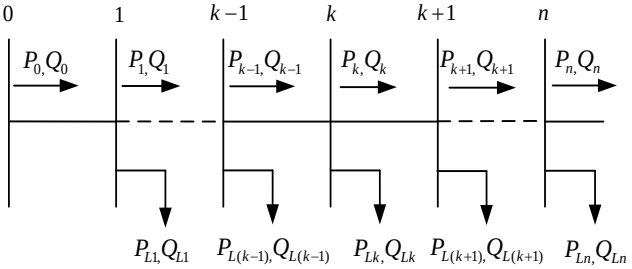

Fig. 1. Single-line diagram of distributed network

According to the Fig. 1, power flow can be recursively calculated as [25]:

$$P_{k+1} = P_k - P_{L(k+1)} - R_{k,k+1}.\frac{(P_k^2 + Q_k^2)}{|V_k|^2} \quad (1)$$

$$Q_{k+1} = Q_k - Q_{L(k+1)} - X_{k,k+1}.\frac{(P_k^2 + Q_k^2)}{|V_k|^2} \quad (2)$$

$$|V_{k+1}|^2 = |V_k|^2 - 2(R_{k,k+1}\cdot P_k + X_{k,k+1}\cdot Q_k) + (R_{k,k+1}^2 + X_{k,k+1}^2)\cdot\frac{(P_k^2 + Q_k^2)}{|V_k|^2} \quad (3)$$

where, P_k and Q_k are the active and reactive power flowing from bus k to bus $k+1$. $P_{L(k+1)}$ and $Q_{L(k+1)}$ represent the active and reactive power, respectively, of the load connected to bus $k+1$. The resistance of the line between the nodes k and $k+1$ is denoted by $R_{k,k+1}$ and the reactance is expressed by $X_{k,k+1}$.

The active power loss of the network can be calculated as:

$$P_{L(k,k+1)} = R_{k,k+1} \cdot \frac{(P_k^{\,2} + Q_k^{\,2})}{|V_k|^2} \tag{4}$$

The total active power loss of the system is equal to the sum of the active power losses between all line segments in the bus. The calculation is shown below:

$$P_T = Min(\sum_{k=0}^{n-1} P_{L(k,k+1)}) \tag{5}$$

B. Deviation of voltage

The voltage deviation can be calculated by Eq. (6).

$$V_d = Min(\sum_{k=1}^{n} (V_k - V_{ref})^2) \tag{6}$$

where, V_k is the voltage of the current node and V_{ref} is the voltage of the balancing node.

The main task of optimizing the configurations of DGs in this paper can be divided into two points as follows.

(1)Single-objective optimal configurations of DGs are Minimizing P_T or V_d as the objective function, and consider the other one as an auxiliary indicator.

(2)Multi-objective optimal configurations of DGs: Pareto optimal solution set is used. P_T and V_d are minimized as the objective function.

C. Factor of sensitivity

In addition, to reduce the calculation complexity and optimize the allocation of limited computational resources, this paper introduces the sensitivity factor into the meta-inspired algorithm and guides for it to find the potential optimal DGs' installation location. The sensitivity factors of active power loss (*PLSF*) and voltage deviation (*VDSF*) are calculated as follows [26]:

$$SenP_k = \frac{\partial P_{k.loss}}{\partial (P+Q)} = \frac{P_0 - P_{cur,k}}{\Delta (P+Q)} \tag{7}$$

$$SenV_k = Vd_0 - Vd_{cur,k} \tag{8}$$

where, $SenP_k$ is the sensitivity factor of active power loss of the k^{th} node, P_0 *and* V_0 are the active power and voltage deviation of the original system. $P_{cur,k}$ is the network loss after subtle changes in network loss of the k^{th} node. $SenV_k$ is the sensitivity factor of voltage deviation at the k^{th} node, and $V_{cur,k}$ is the voltage deviation after subtle changes of power at the k^{th} node.

Arrange *SenP* and *SenV* in descending order, as shown below.

$$SenP_{\max} = sort(SenP_1, SenP_2, ..., SenP_n) \tag{9}$$

$$SenV_{\max} = sort(SenV_1, SenV_2, ..., SenV_n) \tag{10}$$

Normalize *SenP* and *SenV* into the standardized form, the expression is shown below.

$$Nor(x) = \frac{x - x_{\min}}{x_{\max} - x_{\min}} \tag{11}$$

The hybrid sensitivity factor is named *PLVDSF*, which is calculated as follows.

$$SenPV_{\max} = sort(NSenP_1 + NSenV_1, ..., NSenP_n + NSenV_n) \tag{12}$$

where, *NSenP* and *NSenV* are the normalized active power loss sensitivity factor and voltage deviation sensitivity factor.

When P_T is a single target, this paper uses the sensitive factor combined with Eq.(9) of active power loss to guide the selection of the installation positions of DGs. When P_T and V_d are minimized as objective functions, this paper considers Eq. (11) for the combination of *PLSF* and *VDSF* to guide the selection of DG installation location.

D. Constraints

During the power flow calculation, the power of system must satisfy Eq.(1)and Eq.(2), and the voltage magnitude at each node on the system must satisfy Eq. (3).

a: Voltage constraints

For all bus voltages of the system, the amplitude must be located between the constraint ranges, mathematically expressed as follows.

$$V_{Min,k} \le V_k \le V_{Max,k} \tag{13}$$

where, *k* is a non-zero natural number, and the $V_{Max,k}$ is the maximum value of the voltage which is set to 1.05 p.u and the $V_{min,k}$ is the minimum value of the voltage which is set to 0.9 p.u.

b: Current restraint

For the whole system, the current of each branch cannot exceed the following maximum limits. The current restraint is as follows.

$$I_{Min,j} \le I_j \le I_{Max,j} \tag{14}$$

where, *j satisfies j=1,2,…,n-1*, the current of the j^{th} branch is specified as the maximum $I_{Max,j}$, and the minimum current is $I_{Min,j}$.

c: Constraint of generator capacity

To ensure that the DGs can work properly after they are connected to the system, the total active power of the DGs cannot be more than 80% of the active power of the system load. The capacity limits of DG are as follows [27].

$$\sum_{k=1}^{N_{DG}} P_k^{DG} \le 0.8 \times \sum_{k=1}^{n} P_k^L \tag{15}$$

$$\sum_{k=1}^{N_{DG}} Q_k^{DG} \le 0.8 \times \sum_{k=1}^{n} Q_k^L \tag{16}$$

where, *k satisfies k=1,2,3,…,n*, P_k^{DG} and Q_k^{DG} are the active and reactive power of the generator at the *kth* node. P_k^L and Q_k^l are the active and reactive power of the load at the *kth* node, respectively.

d: System power factor constraints

After the DGs are integrated to the network, the power factor of the whole network should be kept within a certain range. The mathematical expression is as follows.

$$pf_{min} \le pf \le pf_{max} \tag{17}$$

The power factor of the whole system is calculated as follows.

$$pf = \frac{\sum_{k=2}^{n} P_k^L - \sum_{k=1}^{N_{DG}} P_k^{DG}}{\sqrt{\left(\sum_{k=2}^{n} P_k^L - \sum_{k=1}^{N_{DG}} P_k^{DG}\right)^2 + \left(\sum_{k=2}^{n} Q_k^L - \sum_{k=1}^{N_{DG}} Q_k^{DG}\right)^2}} \tag{18}$$

In this paper, DGs can be set to only generate active power. The upper and lower limits5 of power factors are pf_{max} and pf_{min}, which are 1 and 0.8 respectively.

III. METHODS

A. Constraint strategy

The PFM primarily combines the violation constraint value and the iteration target value by subjectively adjusting

the size of the penalty coefficient, which reprograms the screening mechanism of the optimisation algorithm, so that the algorithm eliminates the bad solutions that violate the constraint in each iteration. If the value of the penalty coefficient is not appropriate, the algorithm will instead miss the optimal solution, so the selection of the penalty coefficient is crucial. This paper proposes a simplified constraint strategy for the same OADG constraint problem.

Assume that the number of results of each iteration of the objective function is *n*. After each iteration is computed, there exists a solution violation of the constraint whose solution set is defined as *Y*, as follows.

$$Y = \left(y_1, y_2, \cdots, y_n\right) \tag{19}$$

If there exists at least one solution in the solution set y_k, where the solution set *C* is defined to record constraint violations during the iteration, as follows.

$$C = \left(C_1, C_2, \cdots, C_n\right) \tag{20}$$

where, *n* is the number of constraints. The *kth* variable has a constraint record value C_k, the size of which is the fraction of the limit that is exceeded and is defined as follows.

$$C_i = \begin{cases} c_k - c_{\max} & c > c_{\max} \\ c_{\min} - c_k & c < c_{\min} \end{cases} \quad k = \left(1, 2, \cdots, n\right) \tag{21}$$

where, c_k is the current variable size. c_{max} is the upper variable limit and c_{min} is the lower variable limit.

The optimization search process needs to consider all variable violations, and if there are multiple variables violating the constraint, this paper weighs the level of violation by the sum of all constraint violation values. The expression is as follows.

$$C_T = \sum_{i=1}^{n} C_i \tag{22}$$

where, C_T is the total constraint violation value.

For any two individuals *i* and *j*, *i* is superior to *j* if $C_{Ti} < C_{Tj}$. If $C_{Ti} = C_{Tj}$, the result of *i* is superior to *j*, then *i* dominates *j*. Conversely, *j* dominates *i*, which is mathematically defined as follows.

$$\begin{cases} C_{Ti} < C_{Tj} \\ Y_i < Y_j \quad C_{Ti} = C_{Tj} \end{cases} \tag{23}$$

The constraint precedence method eliminates the penalty coefficients, which are parameters with subjective factors, and continuously eliminates the values that violate the constraints during each iteration, finally ensuring that the optimal solution is sought within a reasonable range of values.

B. Salp Swarm Algorithm

The idea of the salp swarm algorithm comes from the aggregation behavior of salps. Salp colonies feed on phytoplankton in the water and move by inhaling and ejecting seawater. Individual salps can be divided into leaders and followers. When the salps are hunting and moving, the leader is in the front position of the group and the followers follow behind [28].

In the SSA algorithm, the position of food source is the target position of all salp individuals, and the position update formula of leaders is as follows.

$$x_j^i = \begin{cases} F_j + c_1((ub_j - lb_j)c_2 + lb_j), c_3 \geq 0.5 \\ F_j - c_1((ub_j - lb_j)c_2 + lb_j), c_3 < 0.5 \end{cases} \tag{24}$$

where, F_j is the position of the food source in the dimensional space, *xi j* is the position of the leader of the i^{th} salp in the j^{th} dimensional space. ub_j and lb_j are the upper and lower limits in the j^{th} dimensional space respectively, and c_1 is the random number. c_2 and c_3 are the two random numbers generated in the [0,1], which determine the orientation and the movement distance of the next position.

The leader's location update is mainly influenced by the food, and c_1 is defined as:

$$c_1 = 2e^{-(4t/\mathrm{T}_{\max})^2} \tag{25}$$

where, *t* is the current number of iterations and T_{max} is the maximum number of iterations.

The location of the followers is updated as follows.

$$x_j^i = \frac{x_j^i + x_j^{i-1}}{2} \tag{26}$$

where, $x_j{}^i$ is the position of the i^{th} follower in dimension *j*. *i satisfies i≥2*.

C. Improved Salp Swarm Algorithm

i. Location update of follower

In the original follower position update, the position of the i^{th} individual is updated based on the midpoint of the coordinates of the i^{th} and $(i\text{-}1)^{th}$ individual positions of the bottlenose sea squirt. This process does not discriminate whether x^i is superior to the original position, and this position update without superiority comparison makes the leading role of the elite bottlenose sea squirt individuals smaller and easy to lose the superior solution. We introduce the Sine Cosine algorithm (SCA) [29] in this paper to update the position of the bottlenose sheath followers, which further enhances the leading role of elite individuals. In order to optimize the exploration and exploitation ability of the bottlenose sheath swarm algorithm, all the followers are operated by sine cosine, and its update formula is as follows.

$$x_i^{t+1} = \begin{cases} x_i^t + r_1 \times \sin(r_2) \times \left| r_3 P_i^t - x_i^t \right|, r_4 < 0.5 \\ x_i^t + r_1 \times \cos(r_2) \times \left| r_3 P_i^t - x_i^t \right|, r_4 \geq 0.5 \end{cases} \tag{27}$$

where, $x_i{}^t$ is the i^{th} dimensional position of the t^{th} generation. r_2 is a random number between 0 and 2π, r_3 is a random number between 0 and 2, r_4 is a random number between 0 and 1, and $P_i{}^t$ is the i^{th} dimensional position of the optimal individual position variable in the t^{th} generation.

The r_1 indicates the region of the next solution location within or outside the current solution and the optimal solution. A small r_1 helps to enhance the local exploitation capability of the algorithm, while a large r_1 helps to improve the global exploration capability, as defined below.

$$r_1 = a - \frac{at}{T_{\max}} \tag{28}$$

where, *a is equal to 2* in this paper.

ii. Location update of Leader

In the original SSA algorithm, the leader is influenced by the position of the food source to update its position. According to Eq.(13), the update of leader's position is influenced by the food source, and the followers then update their position depending on the leader's position.

A single leader limits the search range and global search ability of the whole group, but in fact, there is information sharing among animals living in groups in nature. To reduce the limitation of only the leader guiding the movement of followers, and to enhance the global search ability of the bottlenose sea squirt group. In this paper, we set up decision-makers to simulate the sharing of information in a group of Tarantula, and the decision-makers and the leaders jointly guide the population movement. In this paper, two decision-makers are set to assist the current leader in position updating, and the leader's position is updated as follows.

$$x_j^1 = \begin{cases} F_j + c_1((ub_j - lb_j)c_2 + lb_j) + \beta(dm_j^1 \cos\theta + dn_j^1 \sin\theta), c_3 \geq 0.5 \\ F_j - c_1((ub_j - lb_j)c_2 + lb_j) + \beta(dm_j^1 \cos\theta + dn_j^1 \sin\theta), c_3 < 0.5 \end{cases} \quad (29)$$

θ and β are defined as follows.

$$\theta = 2\pi \cdot rand(0,1) \quad (30)$$

$$\beta = \exp(1 - \frac{t}{T_{\max}}) - 1 \quad (31)$$

where, dm_j^1 and dn_j^1 are the decision makers, θ is the signal factor, and β is the signal transmission coefficient.

In this paper, the improved differential evolution strategy is adopted to update the position of decision-makers as follows.

$$dm_j^i = x_j^i + F_s \times (x_j^{r1} - x_j^{r2}), (i = 1,2) \quad (32)$$

$$dn_j^i = F_j + F_s \times (x_j^{r3} - x_j^{r4}), (i = 1,2) \quad (33)$$

where, F_s is the scaling factor, in this paper, F_s *=0.8,* and r_1, r_2, r_3, r_4 are integers between *[0, N]*.

If there are too many leaders, the randomness of the algorithm will be improved, but the overall stability will be reduced. To balance the randomness and stability of the algorithm, half the salps individuals are treated as leaders in this paper [30].

D. Method flow

The method of sensitivity factor is used in advance to test the installation positions of DGs in this paper. The calculated *PLSF* and *VDSF* are arranged in descending order, and the nodes with the larger sensitivity factor are more likely to be the candidate nodes for the access locations of DGs. This method improves the search efficiency, avoids the problem that the search space increases the computational complexity due to the large dimension, separates the locations and capacity of DGs, and makes the optimized calculation result more accurate. The pseudo-code of the improved ISC-SSA algorithm is shown in Fig. 2.

E. Algorithm Test

In this part, the test results obtained by the ISC-SSA algorithm in four test functions are compared with the SSA algorithm and PSO algorithm respectively, to verify whether the performance of the ISC-SSA algorithm is improved. The six test functions are shown in Fig. 3. The variable dimension of the six test functions is set to 30, the number of iterations is set to 300, three algorithms are tested 20 times. The basic information of six test functions is shown in TABLE I, and the results of the functions are shown in TABLE II.

The experimental tests demonstrate that the ISC-SSA algorithm can obtain superior solutions compared with the SSA algorithm and the PSO algorithm. The improvement of the original SSA algorithm is effective and feasible.

```
begin
calculate SenP and SenV values,
        Obtain the candidate solution set;
1. input: parameters of algorithm(a, F_S , T_max);
2.      Objective function(P_T and V_d)
3.      Initialize the location of population and food source F;
4.      Calculate the value of fitness and constraint violation;
5.      Record restraint violations Constr;
6.        Record the initial optimal individual pbest based on
          Eq. (20) and Eq. (21) ;
7.      Record the global optimal individual gbest, gbest =
          min(pbest);
8.      iter = 1
9.     while iter < T_max
10.           Update the position based on Eq.(26) Through
                Eq.(32);
11.           for i = 1:N (population size)
12.              Objective and constraint calculation;
13.              Record new target and constraint values;
14.              if currentPbest < pbest
15.                 pbest = currentPbest;
16.              end if
17.              currentGbest = min(pbest);
18.              if currentGbest < gbest
19.                 gbest = currentGbest
20.              end if
21.           end for
22.           iter++;
23.     end while
24. output: current optimal solution gbest;
end
```

Fig. 2. Pseudo-code of ISC-SSA algorithm

IV. Simulation and Discussion

This paper will test on IEEE-33, IEEE-69, and IEEE-119 systems and compare the results to other algorithms to demonstrate the superiority of the proposed improved algorithm in practical applications. It is worth stating in particular that to investigate the relationship between P_T and V_d. We will use P_T and V_d as single objectives in 33 and 69 standard test systems to explore whether there is some relationship between them that can make the optimization process optimize one of the objectives and the other objective can also be optimized at the same time. The proposed method will be simulated on a personal computer MATLAB simulation platform equipped with an AMD Ryzen 7 5800H processor, Radeon Graphics@ 3.20GHz and 16GB of RAM.

A. ISC-SSA algorithm on single-objective test systems

a: 33-node test system

The data of the test system comes from [31]. The IEEE-33 system contains 33 nodes, and the reference voltage of the whole system is 12.66 KV. The reference capacity is 100 MW, and the total active loads are 3.715 MW. The reactive loss of the system is 143kVar. The system's total reactive loads and active loss are 2.3MVar and 210.998 KW, with a voltage deviation of 0.1338 p.u. The network topology is shown in Fig. 4.

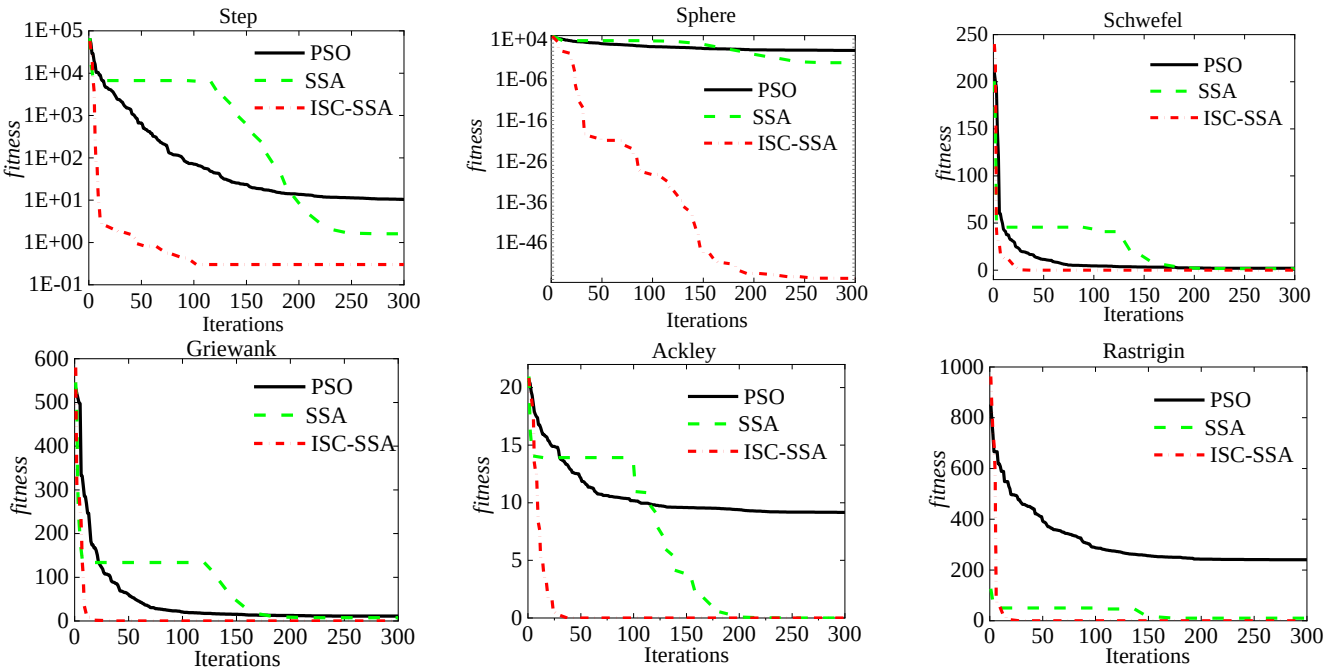

Fig. 3. Iterative diagrams of six test functions

TABLE I
SIX TEST FUNCTIONS

Names	Functions	Ranges
Sphere	$f_1(x)=\sum_{i=0}^{D} x_i^2$	$[-100,100]$
Step	$f_2(x)=\sum_{i=0}^{D}(x_i+0.5)^2$	$[-100,100]$
Schwefel	$f_3(x)=\sum_{i=1}^{D}\lvert x_i\rvert+\prod_{i=1}^{D}\lvert x_i\rvert$	$[-10,10]$
Griewank	$f_4(x)=\sum_{i=1}^{D} x_i^2/4000-\prod_{i=1}^{D}\cos(x_i/\sqrt{i})+1$	$[-600,600]$
Ackley	$f_5(x)=-20\bullet e^{-0.2\sqrt{D^{-1}\sum_{j=1}^{D}x_j^2}}-e^{D^{-1}\bullet\sqrt{\sum_{j=1}^{D}\cos 2\pi\bullet x_j}}+20+e$	$[-32,32]$
Rastrigin	$f_6(x)=\sum_{i=1}^{D}[x_i^2-10\cos(2\pi x_i)+10]$	$[-5.12,5.12]$

TABLE II
RESULTS OF THE THREE ALGORITHMS IN THE TEST FUNCTION

Name	ISC-SSA			SSA			PSO		
	Mean	Best	Worst	Mean	Best	Worst	Mean	Best	Worst
Sphere	4.48E-42	1.87E-55	7.01E-41	1.1914E+00	5.15E-02	1.612E-01	5.3708E+01	1.9811E+01	1.748E+02
Step	4.462E-01	7.35E-01	3.008E-01	1.8651E+00	1.6004E+00	2.3641E+00	5.1354E+01	1.0427E+01	1.3048E+02
Schwefel	4.92E-23	8.35E-28	3.60E-22	3.0595E+00	1.6696E+00	5.475E+00	6.3961E+00	2.0861E+00	1.2708E+01
Griewank	0.00E+00	0.00E+00	0.00E+00	8.7263E+00	7.4482E+00	1.05297E+01	1.7946E+01	1.107E+01	3.0498E+01
Ackley	8.421E-15	8.88E-16	9.234E-13	1.2544E-03	1.3475E-05	1.6422E+00	10.236E+00	9.297E+00	12.853E+00
Rastrigin	0.00E+00	0.00E+00	0.00E+00	12.8456E+00	9.9496E+00	30.8737E+00	224.349E+00	186.64E+00	280.708E+00

Before accessing DGs, *VDSF* and *PLSF* are calculated and normalised according to Eq. (11), and Fig. 5 illustrates the normalised sensitivity factors. Node 18 has the highest sensitivity factor, while nodes 32 and 33 have greater sensitivity factors than their neighbouring nodes. When optimising the IEEE-33 bus, the nodes with larger sensitivity factors can be used as candidate nodes for DGs' accessing; however, the final selected positions of the candidate nodes must be evaluated by optimising the target.

TABLE III contains a variety of cases for the IEEE-33 system that serve to validate the efficacy of the ISC-SSA algorithm in the OADG problem. The cases provide six configurations of connected DGs with the same number of different power factors and the same number of different power factors, respectively.

i. P_T as an objective function

TABLE IV contains the data for various simulation outcomes. Clearly, when DGs with the same power factor access the system, the active power loss (*Ploss*) and voltage deviation (*Vd*) decrease while satisfying the constraints, and the minimal system node voltage can be raised.

Fig. 6 depicts the percentage reduction of *Ploss* and *Vd* in the IEEE-33 test system. By modifying the power factor of the DGs, the DGs become more representative of the actual circumstance, shifting from supplying only active power to supplying both active and reactive power.

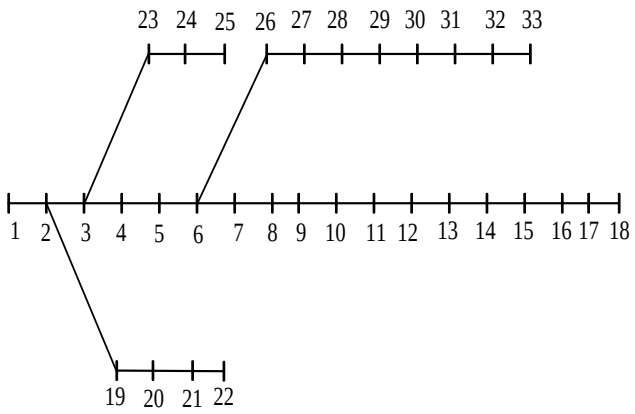

Fig. 4. Topology diagram of IEEE-33

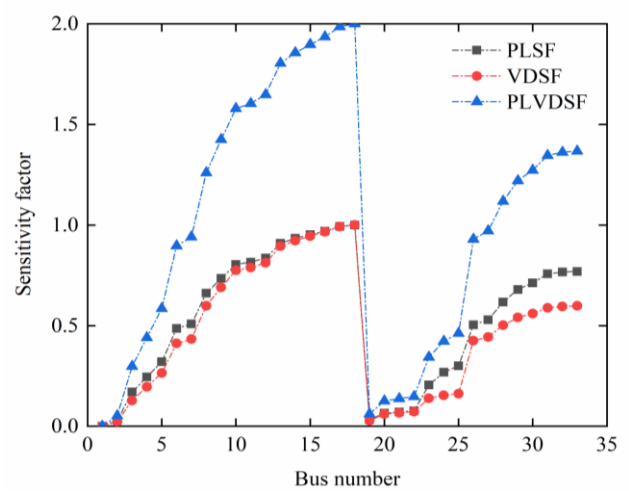

Fig. 5. Sensitivity factor diagram of IEEE-33

Currently, the *Ploss* and *Vd* of the system have decreased significantly. Excitingly, when three DGs with a power factor of 0.95 are connected to the system, the *Ploss* is reduced from the original system's 210.998KW to 12.547KW, a reduction of 94.05%. The *Vd* is decreased from 0.1338 p.u to 0.001433 p.u, representing a decrease rate of 98.93%. In addition, the accessing of DGs enhances the original system's minimum node voltage.

The sensitivity factors of DGs' installation locations are used to guide the OADG problem by selecting larger power loss sensitivity factors, and the *Ploss* of the system is minimised when 3 DGs are configured with the selected DG node locations of 13, 24, and 30, at which point there exists a selected node sensitivity factor that is not exactly for the larger first few, demonstrating that the improved ISC-SSA algorithm has excellent performance. On the one hand, it is the selection of the installation position of DGs, and on the other, it is the capacity of DGs, whereas *PLSF* and *VDSF* measure only the change of individual node position when the capacity is determined. When the capacity and locations of DGs change simultaneously, the optimal installation locations are determined, which may not correspond to the installation locations of DGs with the maximum sensitivity factor.

Ploss decreases as the number of DGs accessing systems increases, given the same factor. Moreover, Fig. 6 reveals that the *Vd* follows the same trend as the *Ploss*, suggesting that the two index parameters may have a positive correlation.

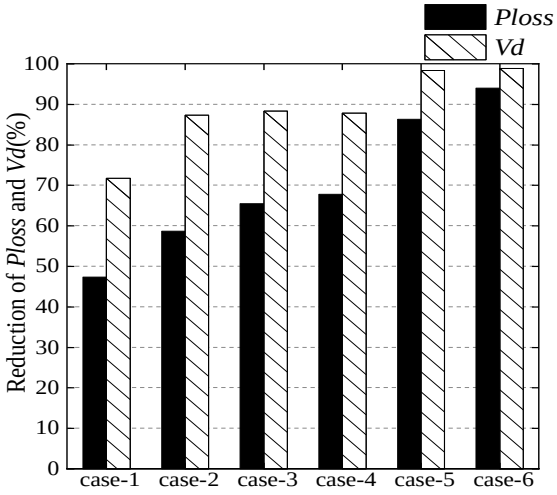

Fig. 6. Percentage reduction of *Ploss* and *Vd* in IEEE- 33

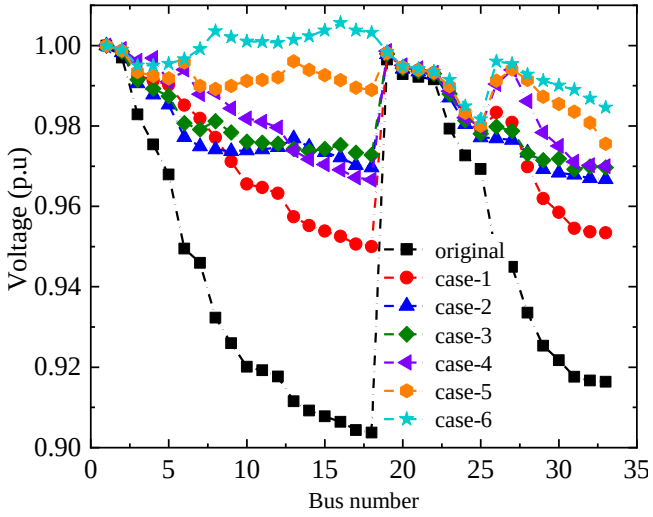

Fig. 7. Bus voltage diagram for different cases in IEEE-33 system

As depicted in Fig. 7, case-6 (3DGs with a power factor of 0.95) has the closest voltage distribution to 1 p.u. Increasing the number of DGs will result in system node voltages that are closer to 1 p.u, with a few nodes exceeding 1 p.u. Overall, the system's voltage distribution has been significantly enhanced.

Fig. 8 depicts the voltage distribution of each node in various circumstances. When DGs with the same power factor but different numbers are connected separately to the system, the voltage distribution of case-5 (2 DGs with a power factor of 0.95) is more uniform than that of case-6 (3 DGs with a power factor of 0.95); However, the nodes voltage of case-6 tends to be closer to 1.0 p.u. There is a substantially reduced median node voltage distribution in case-1 (1 DG with a power factor of 1) than case-4 (1 DG with a power factor of 0.95).

ii. V_d as an objective function

Using *Vd* as the objective function and nodes with large sensitivity factors as candidates, TABLE V displays the simulation results for various DG configurations in the IEEE-33 test system using nodes with large sensitivity factors as candidates. Excitingly, when the ISC-SSA algorithm is used for *Vd* optimisation, the *Vd* reduction rate in case-6 can reach 99.8%, whereas the *Ploss* reduction is limited.

TABLE III
DIFFERENT CONFIGURATIONS IN IEEE-33 SYSTEM

System	Case no.	Number of DGs	Total active power range of DG (MW)	Total reactive power range of DG (MVar)	Factor of power
IEEE-33	case-1	1	0-2.97	-	1
	case-2	2	0-2.97	-	1
	case-3	3	0-2.97	-	1
	case-4	1	0-2.97	0-1.84	0.95
	case-5	2	0-2.97	0-1.84	0.95
	case-6	3	0-2.97	0-1.84	0.95

TABLE IV
SIMULATION RESULTS OF IEEE-33 SYSTEM

Case no.	The optimal size of DGs (MW) (location)	Max and min voltage in p.u (node)	*Ploss* (kW)	Percentage reduction of *Ploss*(%)	*Vd* (p.u)	Percentage reduction of *Vd*(%)
original	-	1(1) 0.9037(18)	210.998	0	0.1338	0
case-1	2.5904(6)	1(1) 0.950009(18)	110.032	47.37	0.037731	71.80
case-2	0.851(13) 1.1574(30)	1(1) 0.966735(33)	87.169	58.68	0.016973	87.31
case-3	0.7946(13) 1.078(24) 1.0482(30)	1(1) 0.969226(31)	72.796	65.49	0.015538	88.39
case-4	2.5537(6)	1(1) 0.966618(18)	67.87	67.83	0.01631	87.81
case-5	1.1191(30) 0.7745(13)	1(1) 0.975555(33)	28.813	86.34	0.002218	98.34
case-6	0.7099(13) 1.16(24) 0.996(30)	1.005628(16) 0.981656(25)	12.547	**94.05**	0.001433	**98.93**

As shown in Fig. 9 when *Vd* is minimised as the objective function, *Vd* decreases progressively as the number of DGs increases, but *Ploss*, the reference indicator, no longer decreases. Specifically, *Vd* in case-1 is considerably lower than in case-2, whereas *Ploss* in case-2 is greater than in case-1. The voltage distribution curve obtained with *Vd* as the objective function is depicted in Fig. 10. Clearly, the proposed approach can still enhance the voltage performance of the original system. Specifically, the voltage distribution of case-6 is more uniform and the system voltage quality is improved.

To demonstrate the benefit of ISC-SSA in optimising *Ploss*, the simulation results of case-3 are contrasted to those of the other algorithms in TABLE VI, when the system is connected to three DGs at nodes 13, 24, and 30, respectively. The *Ploss* obtained by the ISC-SSA algorithm is 72.796 KW, which is greater than the *Ploss* obtained in the literature [24] using PSO, MTLBO, GWO, and Jaya algorithms with the improvement of 5.17%, 3.51%, 0.61%, and 0.08%, respectively. In terms of active power loss optimisation, the ISC-SSA algorithm outperforms both HHO [32] and NNA [33]. This demonstrates the significant advantage of the ISC-SSA algorithm for OADG problem resolution.

b: 69-node test system

The data for the test system comes from [34]. The IEEE-69 node network contains 69 nodes and 68 branches. The reference voltage of the entire system is 12.66 KV and the reference capacity is 100 MW. The total active load is 3.80 MW, and the total reactive load is 2.69MVar, with a voltage deviation of 1.8359 p.u. The system's reactive loss and active loss are 102.14kVar and 224.947 KW. The topology of the network is shown in Fig. 11. The IEEE-69 test system is more difficult to understand than its predecessor, the IEEE-33 test system. The target search space expands from 33 nodes to 69 nodes, the size of the search space grows, and the complexity of the search rises by more than 9.6 times.

The approach was used to validate that the upgraded ISC-SSA algorithm is applicable to other progressively complicated scenarios by applying it to the IEEE-69 bus system. Calculations and normalisations are performed on the *PLSF* and *VDSF* before the system is connected to the DGs.

Fig. 12 demonstrates that the majority of nodes have high sensitivity values, such as nodes 18, 61, 63, etc. However, there are some nodes in the system that have relatively low sensitivity, such as nodes 29, 37, etc. The nodes with larger sensitivity factors are used as access location candidates for DGs, and the ISC-SSA algorithm optimises the target. The configurations of DGs in the IEEE-69 system are listed in TABLE VII.

i. P_T as the objective function

The outcomes of six cases with diverse DG configurations in the IEEE-69 system are presented in TABLE VIII. Appropriate configurations of DGs on the 69-bus system can reduce Ploss and Vd. Case-9's loss reduction reaches 69.14%, while Vd is reduced by 94.87%. In case-11, Ploss is reduced to 13.1658 kW and Vd is reduced to 0.003127 p.u, and there are only two generators configured, which is more cost-effective than case-9 in the application, indicating that DGs injecting both active and reactive power is significantly superior to injecting only active power.

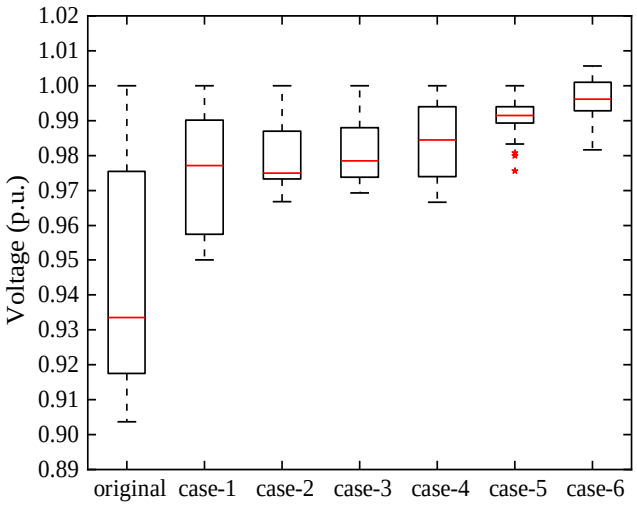

Fig. 8. Voltage box line diagram for different cases in the IEEE-33 system

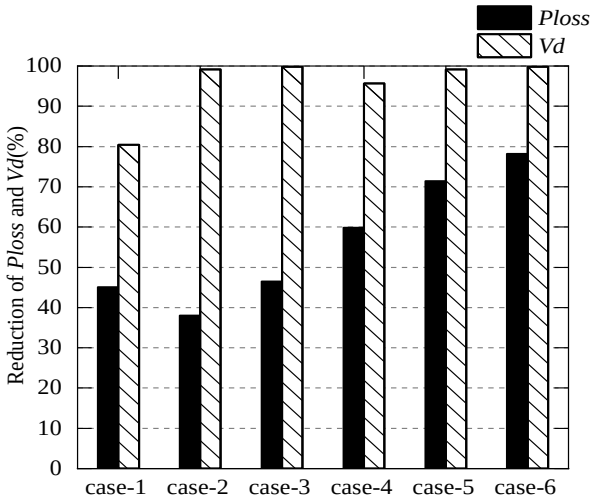

Fig. 9. Percentage reduction of *Ploss* and *Vd* when minimizing *Vd*

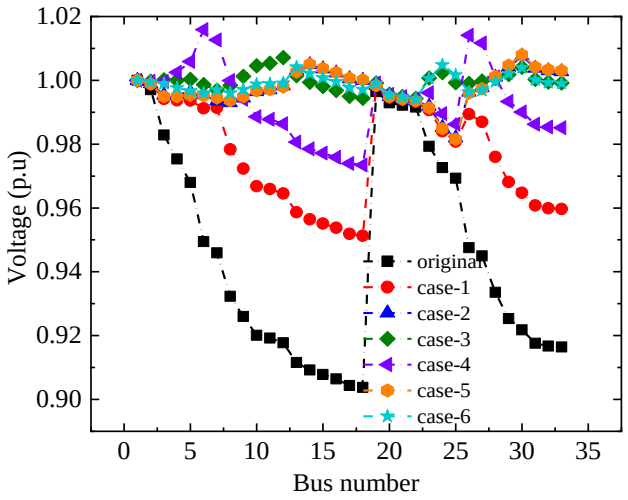

Fig. 10. Voltage distribution of nodes when minimizing *Vd*

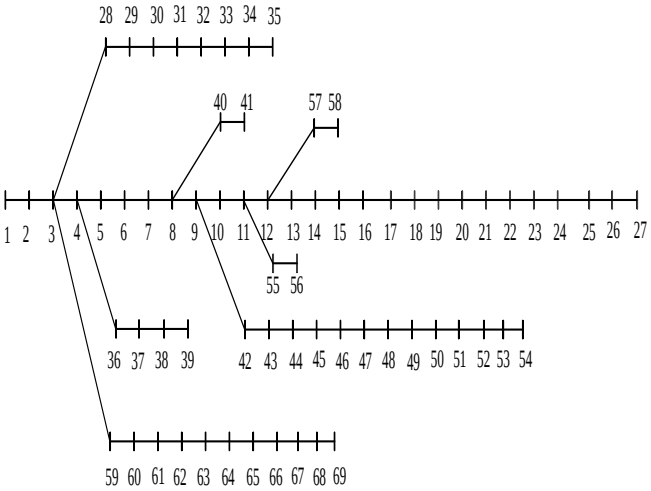

Fig. 11. Topology diagram of IEEE-69

TABLE V
RESULTS OF THE 33-NODE SYSTEM TO OPTIMIZE VD

Case no.	The optimal size of DGs (MW) (location)	V_{max} and V_{min} p.u. (node)	*Vd* (p.u.)	Percentage reduction of *Vd*(%)	*Ploss* (KW)	Percentage reduction of *Ploss*(%)
original	-	1(1) 0.9037(18)	0.1338	0	210.998	0
case-1	2.972(7)	1(1) 0.9513(18)	0.026178	80.44	115.9881	45.0288
case-2	0.851(13) 1.1574(30)	1.0076(30) 0.9819(25)	0.001119	99.16	130.8917	37.965
case-3	0.7946(13) 1.078(24) 1.0482(30)	1.0071(12) 0.9943(22)	0.000295	99.78	112.9009	46.492
case-4	2.5537(6)	1.0159(6) 0.9734(18)	0.005781	95.68	84.79666	59.812
case-5	1.1191(30) 0.7745(13)	1.008(30) 0.9815(25)	0.001172	99.12	60.36186	71.392
case-6	0.7099(13) 1.16(24) 0.996(30)	1.0049(24) 0.9941(22)	0.000262	**99.80**	46.12227	78.141

It is worth illustrating that the *Ploss* is reduced by 89.72% in case-10(1 DG with a power factor of 0.95), which is better than the cases of DGs providing only active power, with a lowest node voltage of 0.9724 p.u. The voltage deviation is reduced by 88.07% compared to the original system, while the voltage deviation in case-8 is reduced by 89.55%, which is significantly better than case-10. This suggests that for *Ploss* and *Vd* optimisation, the location and capacity of DGs play a crucial role in achieving the system optimisation goals.

TABLE VI
COMPARISON OF MULTIPLE ALGORITHMS IN A 33-NODE STANDARD SYSTEM

Algorithm	Optimal location	Optimal size of DGs(MW)	*Ploss* (KW)	Percentage reduction of *Ploss*(%)
ISC-SSA	13 24 30	0.7965 1.0833 1.0596	**72.796**	**65.49**
PSO	10 30 27	0.9200 0.8390 0.7450	83.72	60.32
MTLBO	23 32 15	1.0660 0.8470 0.8850	80.22	61.98
GWO	12 25 30	0.9550 1.0330 1.018	74.1	64.88
JAYA	29 25 12	0.9210 0.7950 1.1100	76.66	63.67
HHO	14 24 30	0.7456 1.0230 1.136	72.98	65.41
NNA	14 24 29	0.9290 1.0090 0.8880	75.762	64.09

Fig. 13 shows the percentage reduction of *Ploss* and *Vd* of the ISC-SSA algorithm in the IEEE-69 bus system under different configurations of DGs. The *Ploss* of the whole system after a single DG (case-7) connected to the IEEE-69 system is 83.18KW, which is more than half of the total Ploss. Case-9 shows the *Ploss* of 70.01KW when 3 DGs are connected at the same time, which is improved compared with case-7, but its reduction is limited and the effect is weakened, and the phenomenon is consistent with the IEEE-33 system. Concerning the *Vd* index, we can see from the graph that the *Ploss* and *Vd* are positively correlated in the case of DGs with the same power factor. Combined with the relationship between them in the IEEE-33 test system, we can determine that with *Ploss* as the target, there may be some positive correlation between *Ploss* and *Vd* based on DGs with the same power factor.

From Fig. 14 and Fig. 15, it shows that compared to the original system compared to the original system, the introduction of DGs altered the current distribution and increased the voltage at each node. Compared to case-10, the voltage of each node in case-9 is approximately 1.0 p.u. The voltage distribution of the nodes in case-10 is more uniform. However, case-10's *Ploss* is less than case-9's and case-10's *Vd* is greater than case-9's. The results indicate that there is no correlation between *Ploss* and *Vd* when both are targeted simultaneously.

ii. V_d *as an objective function*

With *Vd* as the objective function, the simulation results for various DG configurations in the IEEE-69 test system are presented in TABLE IX. It can be seen that when the ISC-SSA algorithm is used to optimise *Vd*, the *Vd* reduction rate in case-12 can be as high as 99.71%, the *Ploss* reduction rate can be as high as 93.7%, and the minimum voltage of the node is 0.9943 p.u.

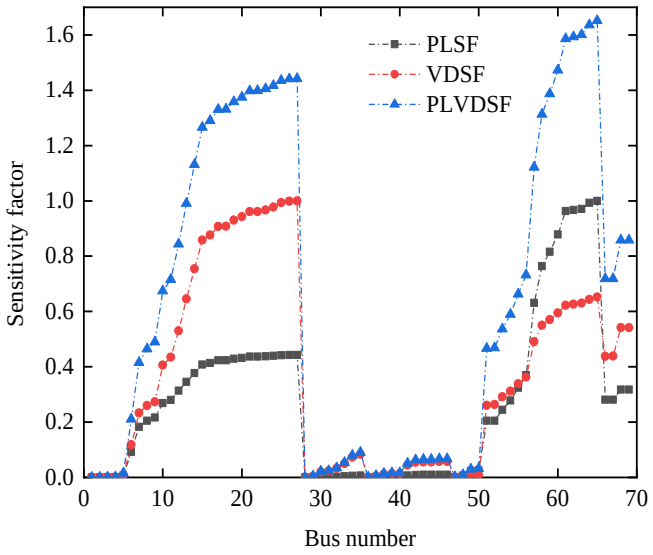

Fig. 12. Sensitivity factor diagram of IEEE-69

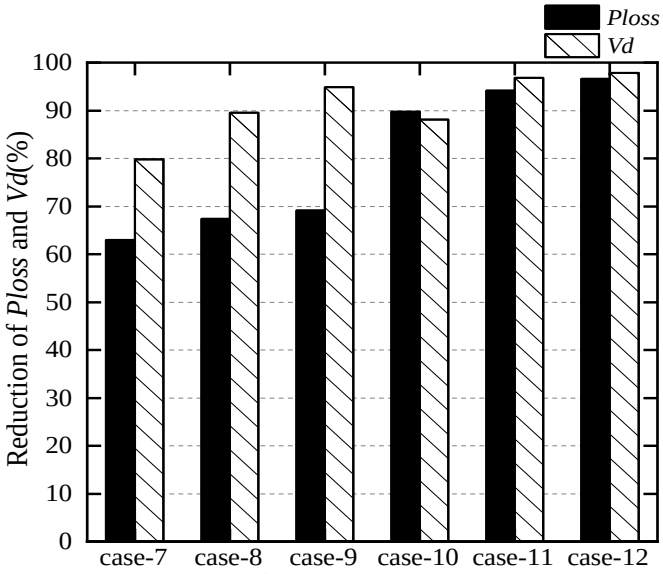

Fig. 13. Percentage reduction of *Ploss* and *Vd* in IEEE-69

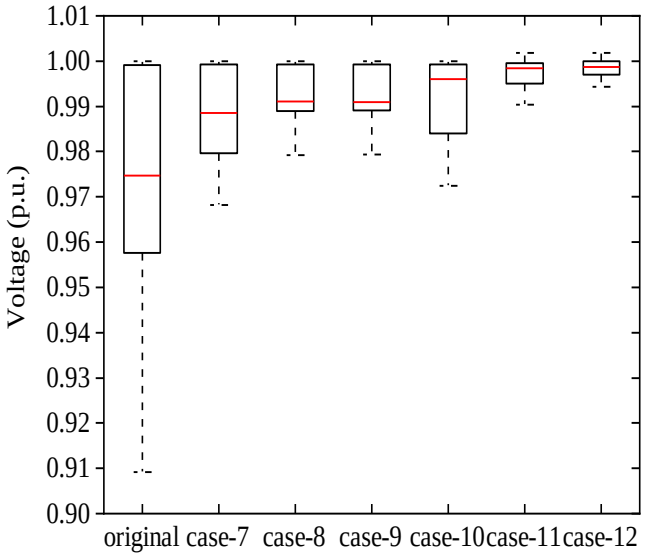

Fig. 14. Voltage box line diagram for different cases in the IEEE-69

TABLE VII
CONFIGURATION OF DGS IN IEEE-69 SYSTEM

System	Case no.	Number of DGs	Total active power range of DG (MW)	Total reactive power range of DG (MVar)	Factor of power
IEEE-69	case-7	1	0-3.04	-	1
	case-8	2	0-3.04	-	1
	case-9	3	0-3.04	-	1
	case-10	1	0-3.04	0-2.15	0.95
	case-11	2	0-3.04	0-2.15	0.95
	case-12	3	0-3.04	0-2.15	0.95

TABLE VIII
SIMULATION RESULTS OF IEEE-69 SYSTEM

Case no.	Active power of DGs (MW) (node)	V_{max} and V_{min} p.u (node)	*Ploss* (KW)	Percentage reduction of *Ploss*(%)	*Vd* (p.u)	Percentage reduction of *Vd*(%)
original	-	1(1) 0.9092(65)	224.947	0	0.0993	0
case-7	1.8691(61)	1(1) 0.9682(27)	83.18	63.02	0.020074	79.78
case-8	0.5055 (20) 1.7585 (69)	1(1) 0.9792(65)	73.2702	67.43	0.010375	89.55
case-9	0.5495 (17) 1.3854(61) 0.3792 (63)	1(1) 0.9794(65)	69.4044	69.14	0.005097	94.87
case-10	1.8314 (61)	1(1) 0.9724(27)	23.135	89.72	0.011846	88.07
case-11	1.6731 (62) 0.6309(69)	1.0018(12) 0.9903(27)	13.1658	94.15	0.003127	96.85
case-12	0.4720 (17) 1.2947 (61) 0.4791(63)	1.0018(18) 0.9943(50)	7.675	**96.59**	0.002154	**97.83**

TABLE IX
SIMULATION RESULTS OF IEEE-69 SYSTEM TO MINIMIZE *VD*

Case no.	The optimal size of DGs (MW) (location)	V_{max} and V_{min} p.u (node)	*Vd* (p.u)	Percentage reduction of *Vd*(%)	*Ploss* (KW)	Percentage reduction of *Ploss*(%)
original	-	1(1) 0.9092(65)	0.0993	0	224.947	0
case-7	2.6426 (62)	1.0087(62) 0.9727(27)	0.011925	87.99	106.002	52.88
case-8	0.9189 (15) 1.8959 (62)	1.005(15) 0.9862(65)	0.001984	98.00	79.045	64.86
case-9	0.6795 (17) 1.0757(61) 1.17927(63)	1(1) 0.9933(69)	0.000691	99.30	81.959	63.57
case-10	1.9306(61)	1.0108(61) 0.9748(27)	0.010072	89.86	34.551	84.64
case-11	1.5845(62) 1.5117(69)	1.009(11) 0.9943(50)	0.000832	99.16	18.118	91.95
case-12	0.5049(17) 0.4418(61) 1.2062(63)	1.0032(63) 0.9943(50)	0.000286	**99.71**	14.152	**93.71**

As can be seen from Fig. 16 with *Vd* minimized as the target and *Ploss* as the reference index, *Vd* gradually decreases with the increase in the number of DGs for the same power factor. *Ploss* and *Vd* do not satisfy the positive correlation shown in case-8 and case-9. Combined with the conclusions drawn from the IEEE-33 test system, it can be determined that there is no positive correlation between *Ploss* and *Vd.*

Since *Ploss* and *Vd* do not have a positive correlation, it is difficult to acquire the minimum value of both simultaneously during optimisation, and it is unreliable to consider any one of the sensitivity factors as a factor in determining the location of DGs. In the following section, this paper will incorporate the *PLSF* and *VDSF* for multi-objective optimisation.

As shown in Fig. 17 with *Vd* as the objective function, the proposed method substantially enhances the voltages at each node, and the voltage values at some nodes exceed the reference voltage values while remaining within the voltage limits. The ISC-SSA algorithm substantially enhances the IEEE-69 system's voltage deviation and worst-case voltage.

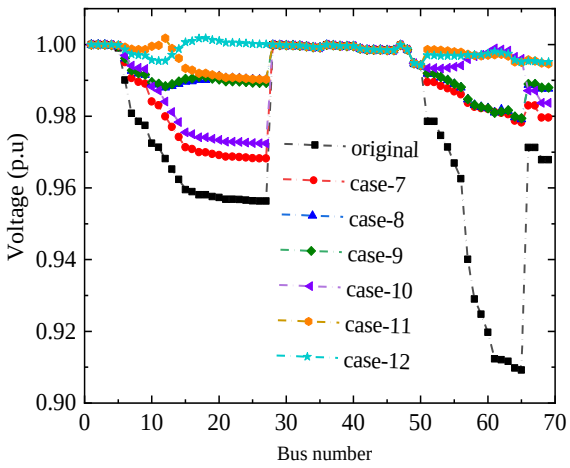

Fig. 15. Bus voltage diagram for different cases in IEEE-69 system

TABLE X displays the outcomes of the comparison between various papers published on the IEEE-69 network in recent years. The ISC-SSA algorithm proposed in the paper is superior to the method described in [35-37] because the difference in *Ploss* for identical configurations of DGs is not statistically significant when compared to the algorithm in [38-40]. The results demonstrate that the ISC-SSA proposed in this paper outperforms other algorithms in reducing active power losses.

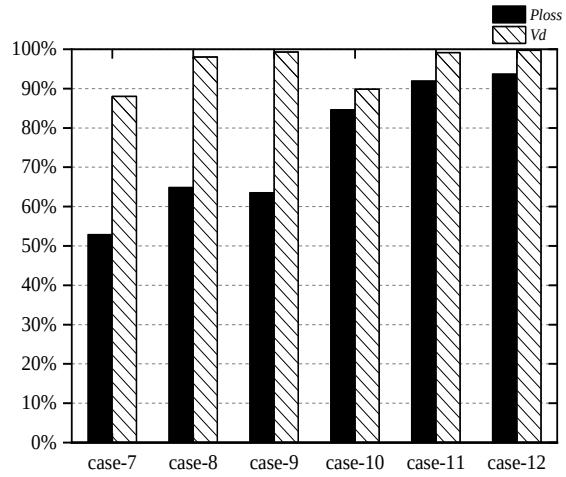

Fig. 16. Percentage reduction graph of *Ploss* and *Vd* for IEEE-69 system

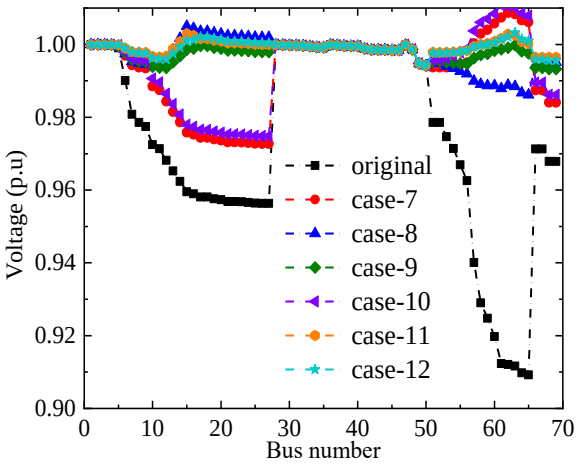

Fig. 17. Voltage distribution in IEEE-69 system when minimizing *Vd*

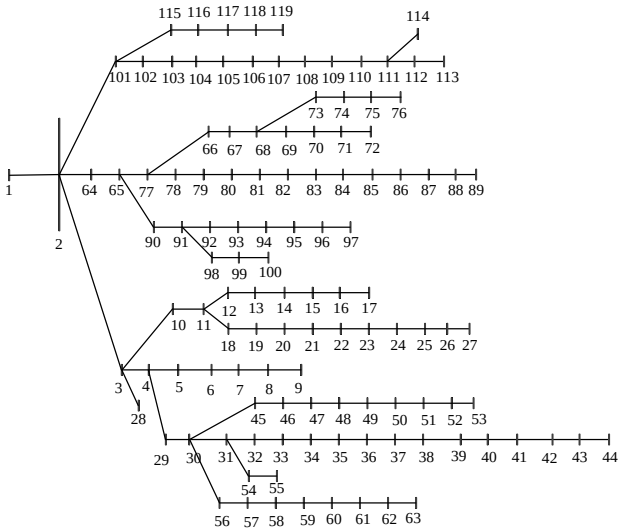

Fig. 18. Topology diagram of IEEE-119

c: 119 node test system

The data of the system comes from [6]. This system contains 119 nodes and 118 branches. The network topology is shown in Fig. 18. The reference voltage of the whole system is 12.66 KV and the reference capacity is 100 MW. The network has a total active load of 22.71 MW and a total reactive load of 17.04MVar. The *Ploss* of the whole network is 978.1 KW and the reactive loss is 718.8KVar.

TABLE X
COMPARISON RESULTS OF DIFFERENT ALGORITHMS IN IEEE-69 SYSTEM

Algorithm	Optimal location	Optimal size of DGs(MW)	*Ploss*(KW)	Percentage reduction of *Ploss*(%)
ISC-SSA	6 18 61	0.7965 1.0833 1.0596	**69.404**	**69.15**
OTCDE[35]	11 18 61	0.5268 0.3803 1.7189	69.428	69.14
CTLBO[36]	11 18 61	0.5268 0.3796 1.7190	69.4284	69.14
SFSA[37]	11 18 61	0.5273 0.3805 1.7198	69.428	69.14
MOCDE[38]	11 19 61	0.5588 0.4115 1.8499	70.259	68.77
TLBO[39]	15 61 63	0.5919 0.8188 0.9003	72.410	67.81
QOSIMBO-Q[40]	9 18 61	0.8336 0.4511 1.500	71.000	68.44

Appling ISC-SSA algorithm into the IEEE-119 system to prove the validation of merit-seeking capability. Before configuring the DGs, the *PLSF* and *VDSF* of the system are calculated and normalized, and the normalized sensitivity factors are shown in Fig. 19. It can be seen from the figure that the sensitivity factors at nodes 40, 64, and 70, 85, 111, etc. are relatively large and can be used as candidate nodes. Compared with the IEEE-69 system, the IEEE-119 system becomes more complex, with a nearly 1-time increase in the range of node location parameters. The complexity of the optimization problem increases by a factor of 5.23 for the 3

DGs configuration. In addition, the configurations of DGs in the IEEE-119 system are shown in TABLE XI.

TABLE XII displays the simulation results of the IEEE-119 system with *Ploss* as the target. In the meantime, the table provides six combined configuration schemes derived from SSA, PSO, and ISC-SSA algorithms, while Fig. 20 depicts the node voltage distributions for various configuration schemes. Fig. 21 depicts the reduction rates of *Ploss* and *Vd* for various configurations. Compared to the other two test systems, there are fewer case studies on OADG optimisation of 119-node networks, as indicated by the relevant literature. Encouragingly, the configuration scheme with four DGs obtained by the ISC-SSA algorithm in this paper effectively reduces *Ploss* by 66.7% and *Vd* by 78.62%, resulting in a significant improvement in the voltage distribution. The results indicate that ISC-SSA performs better in complex systems than the SSA and PSO algorithms.

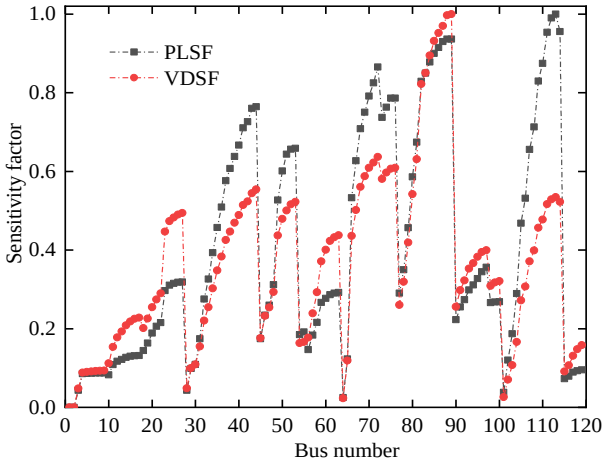

Fig. 19. Sensitivity factor diagram of IEEE-119

Fig. 22 depicts the convergence trajectories of the SSA, PSO, and ISC-SSA algorithms for the IEEE-119 system with minimum *Ploss* as the objective function. Compared to the other two algorithms, the ISC-SSA algorithm exhibits a significant improvement in searching precision.

B. MOISC-SSA on multi-objective test systems

As the minimum *Ploss* and minimum *Vd* metrics have been previously simulated on the three different sizes of standard systems with different DG configurations respectively. The simulation of the multi-objective problem will be conducted in IEEE-33 and IEEE-69 test systems in this part, and the configurations of the above two test systems are shown in TABLE XIII, where the power factor is set to 0.8. Since the same test system is used for this subsection and the single-target problem, the range of values for each variable is the same, but considering the complexity of the multi-objective problem and the smoothness of the Pareto Frontiers, the number of populations is set to 100 here, and the maximum number of iterations on IEEE-33 and IEEE-69 is 300.

To get the best compromise (BCS) obtained by MOISC-SSA for both *Ploss* and *Vd* as optimization objectives, the simulation results of the corresponding configurations with *Ploss* and *Vd* as single objectives are presented in TABLE XIV, which provide some reference for the multi-objective simulation results on the same test systems.

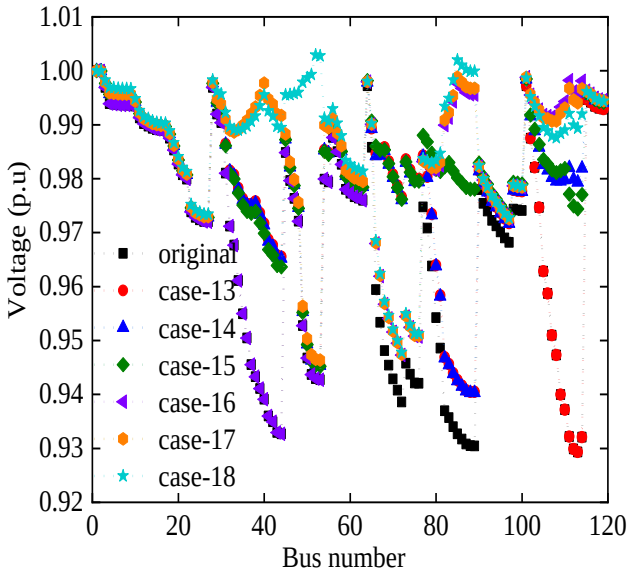

Fig. 20. Voltage distribution for different cases in the IEEE-119 system

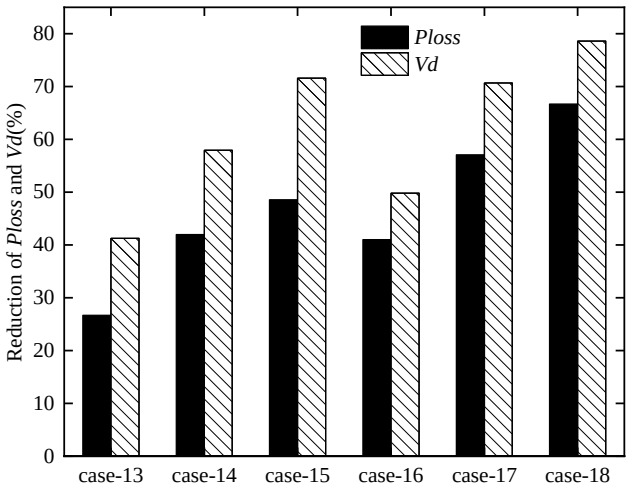

Fig. 21. Percentage reduction graph of *Ploss* and *Vd* for IEEE-119 system

a: IEEE-33 Test System

Among the multiple solutions in the obtained PFs, there are three OADG solutions that deserve special consideration: the one with the lowest *Ploss*, the one with the lowest *Vd*, and the optimal BCS solution that combines *Ploss* and *Vd*. TABLE XV lists the minimal *Ploss*, minimum *Vd*, and optimal compromise solution for each configuration.

Combining the sensitivity factors in Fig. 5 those with greater values in *PLVDSF* are used as candidate nodes for DG access locations, such as points 6, 18, 30, 32, etc. From TABLE XIV, the results obtained from the single-objective optimization significantly optimize the corresponding indexes obtained from the simultaneous multi-objective optimization. In particular, the BCS obtained by the MOISC-SSA algorithm is closer to the optimization results obtained with *Ploss* as the objective when 1 DG is connected to the test system.

Fig. 23 shows the node voltages for different DG configurations for multiple targets. It is evident that each of the obtained BCS schemes is advantageous for increasing the node voltages of the original distribution network.

TABLE XI
CONFIGURATIONS OF DGS IN IEEE-119 SYSTEM

System	Case no.	Number of DGs	Total active power range of DG (MW)	Total reactive power range of DG (MVar)	Factor of power
IEEE-119	case-13	2	0-18.17	-	1
	case-14	3	0-18.17	-	1
	case-15	4	0-18.17	-	1
	case-16	2	0-18.17	0-13.63	0.95
	case-17	3	0-18.17	0-13.63	0.95
	case-18	4	0-18.17	0-13.63	0.95

TABLE XII
SIMULATION RESULTS OF DIFFERENT DGS' CONFIGURATIONS IN IEEE-119 SYSTEM

Algorithm	Number, size of DGs	Factor of power	Number, size of DGs (MW)	*Ploss* (KW)	Percentage reduction of *Ploss*(%)	*Vd* (p.u)	Percentage reduction of *Vd*(%)	V_{min} p.u (node)
original	-	-	1(1) 0.9093(113)	978.1	0	0.1875	0	0.9293(113)
ISC-SSA	2	0.95	2.9012(81) 2.7528(111)	577.224	**40.99**	0.0941	**49.81**	0.9327(44)
		1	3.4922(38) 3.5883(68)	717.046	**26.69**	0.1102	**41.23**	0.9293(113)
SSA		0.95	1.9046(85) 2.7409(111)	599.908	38.67	0.098923	47.24	-
		1	1.9849(85) 2.7797(110)	731.556	25.21	0.111685	40.43	
PSO		0.95	2.1242(85) 2.1241(110)	609.50	37.69	0.097576	47.96	
		1	1.9260 (85) 2.8657(111)	731.475	25.21	0.1119	40.32	
ISC-SSA	3	0.95	2.9876(40) 1.9363(85) 2.5515(111)	419.914	**57.07**	0.05496	**70.69**	0.9464(53)
		1	3.4601(38) 3.5304(68) 2.8787(111)	567.590	41.97	0.07891	57.91	0.9403(89)
SSA		0.95	2.3058(39) 2.2826(85) 2.2412(111)	443.468	54.66	0.056088	70.09	-
		1	3.5655(38) 3.2654(68) 2.9865 (110)	569.012	41.82	0.079849	57.41	
PSO		0.95	2.2356(40) 2.2003(85) 2.2277(111)	443.42	54.67	0.055658	70.32	
		1	3.6491(38) 3.3597(68) 3.1619 (110)	568.431	41.88	0.078927	57.906	
ISC-SSA	4	0.95	2.8765(40) 1.4092(52) 2.0859(85) 2.2904(111)	325.67	**66.70**	0.040085	**78.62**	0.9459(72)
		1	3.2847(38) 3.0327(68) 1.9542(83) 3.0286(110)	503.130	48.56	0.05328	71.584	0.9452 (53)
SSA		0.95	2.6775(40) 2.6775(64) 3.1160(73) 2.6775(111)	355.97	63.61	0.043855	76.61	-
		1	2.9943(40) 4.5298(64) 1.9691(85) 2.8966(110)	609.38	37.70	0.077598	58.61	
PSO		0.95	2.8709(40) 2.7176(64) 2.8344(73) 2.8273(111)	373.147	61.85	0.053766	71.32	
		1	2.9051(38) 2.8282(68) 1.7599(85) 3.4909(110)	512.444	47.61	0.055309	70.50	

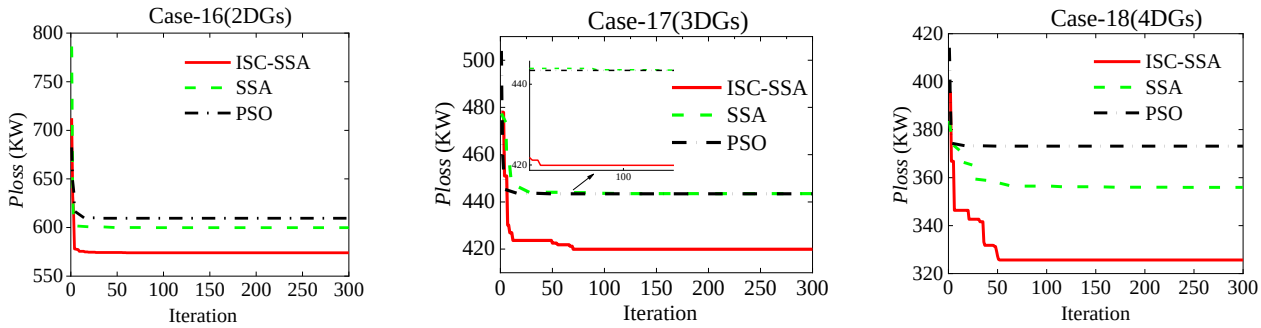

Fig. 22 Iterative curves of active power loss in IEEE-119 systems

TABLE XIII
CONFIGURATIONS OF DGS IN THE MULTI-OBJECTIVE TEST SYSTEM

System	Number of DGs	Total active power range of DG (MW)	Total reactive power range of DG (MVar)	Power factor
IEEE-33	1 2	0-2.97	0-1.84	0.8
IEEE-69	1 2	0-3.04	0-2.15	

TABLE XIV
SIMULATION RESULTS IN CASE-33 AND CASE-69 TEST SYSTEM

Target	System	Number, size of DGS	Number, size of DGs (MW) (location)	*Ploss* (KW)	Percentage reduction of *Ploss*(%)	*Vd* (p.u)	Percentage reduction of *Vd*(%)
Ploss	case-33	1	2.5603(6)	67.86896	67.83	0.016289	87.83
		2	1.1927(30) 0.7836(14)	28.760	**86.37**	0.001700	**98.73**
	case-69	1	1.8251 (61)	23.1355	89.72	0.011837	88.08
		2	1.6901(62) 0.7421(69)	11.6096	97.84	0.002084	97.90
Vd	case-33	1	2.972(6)	75.077	64.42	0.007574	**94.34**
		2	1.486(30) 1.0440(13)	41.764	80.21	0.001108	**99.17**
	case-69	1	1.9619(61)	37.993	83.11	0.010014	89.92
		2	1.5933(61) 1.1140 (69)	18.934	91.58	0.000711	99.28

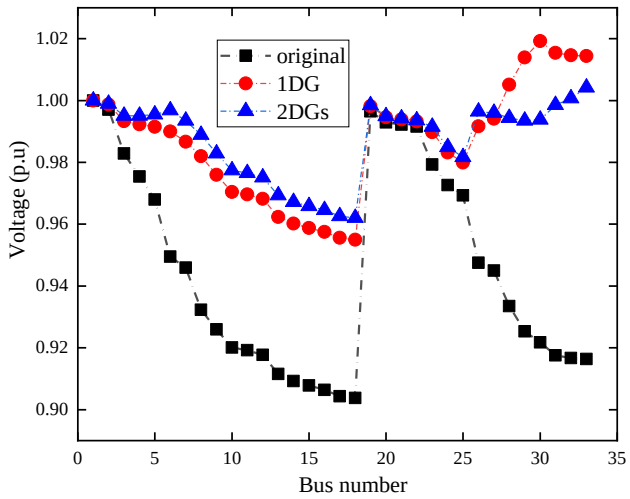

Fig. 23.Voltage diagram for multi-target configurations in IEEE-33 system

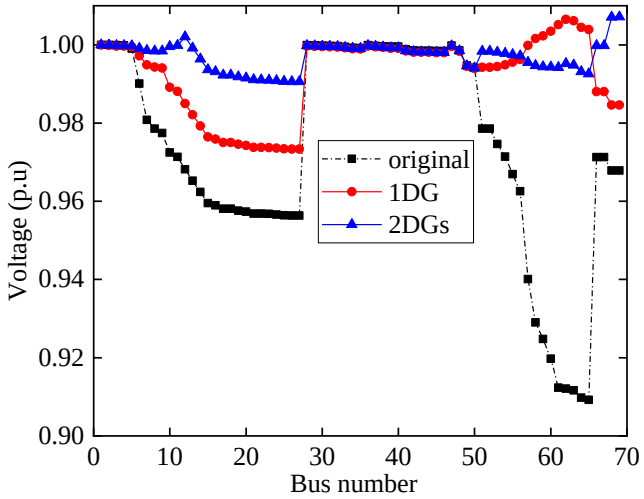

Fig. 24. Voltage diagram for multi-target configurations in IEEE-69 system

Fig. 25 shows the multi-objective PF curves in the IEEE-33 test system. MOISC-SSA algorithm obtains uniformly distributed PFs for both one DG and two DGs configured on the 33-node network. It is worth stating that multiple configuration schemes that constitute the PF sets are feasible solutions for achieving zero-constraint violation.

b: IEEE-69 Test System

TABLE XVI lists the optimal compromise solution in the IEEE-69 system for different configurations. The nodes with larger values in the *PLVDSF* are used as candidates for access locations of DGs, such as points 18, 19, 62, 64, 69, etc. Compared with the IEEE-33 test system, the BCS

obtained by the MOISC-SSA algorithm in the IEEE-69 test system is closer to the optimization results obtained during single-objective optimization, especially when two DGs are connected to the test system, the *Ploss* reduction rate is as high as 92.3% and the *Vd* reduction rate is as high as 98.59%. Fig. 24 illustrates the node voltages for different DG configurations with multiple targets.

In addition, Fig. 26 also depicts the multi-objective PF curves in the IEEE-69 test system. Meanwhile, The MOISC-SSA algorithm obtains more uniformly distributed PFs in the case of both one DG and two DGs configured on the 69-node network.

TABLE XV
MULTI-OBJECTIVE CONFIGURATION SCHEME FOR IEEE-33 TEST SYSTEM

case-33	BCS(*Ploss*/*Vd*)	Minimal *Ploss*/*Vd*	*Ploss*/ Minimal *Vd*
1DG	73.555/0.0169	68.645/0.0198	82.502/0.0155
Reduction percentage	**65.14%/87.37%**	67.47%/85.20%	60.90%/88.42%
Capacity (location) of DGs	1.98888 (30)	1.77844 (30)	2.20497(30)
2DG	41.071/0.0104	41.059/0.0105	41.096/0.0102
Reduction percentage	81.74%/89.53%	81.75%/89.43%	81.73%/89.73%
Capacity (location) of DGs	1.486(32) 0.81503(6)	1.486(32) 0.80623(6)	1.486(32) 0.82321(6)

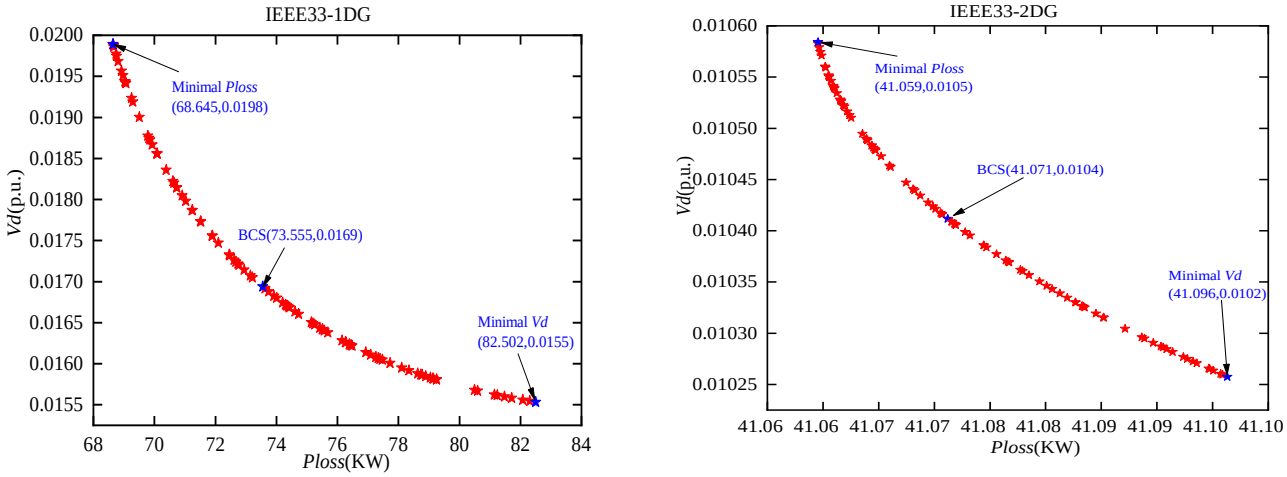

Fig. 25. PF curves in the IEEE-33 test system

TABLE XVI
MULTI-OBJECTIVE CONFIGURATION SCHEME FOR IEEE-69 TEST SYSTEM

case-69	BCS(*Ploss*/*Vd*)	Minimal *Ploss*/*Vd*	*Ploss*/ Minimal *Vd*
1DG	27.003/0.0111	25.574/0.0125	31.322/0.0106
Reduction percentage	80.53%/91.70%	87.88%/90.66%	85.16%/92.08%
Capacity (location) of DGs	1.93965(62)	1.77431(62)	2.1080(62)
2DG	17.317/0.0014	14.599/0.0032	23.346/0.00086
Reduction percentage	**92.30%/98.59%**	93.51%/96.78%	89.62%/**99.13%**
Capacity (location) of DGs	1.51676(62) 0.95533(69)	1.51676(62) 0.71906(69)	1.51676(62) 1.18639(69)

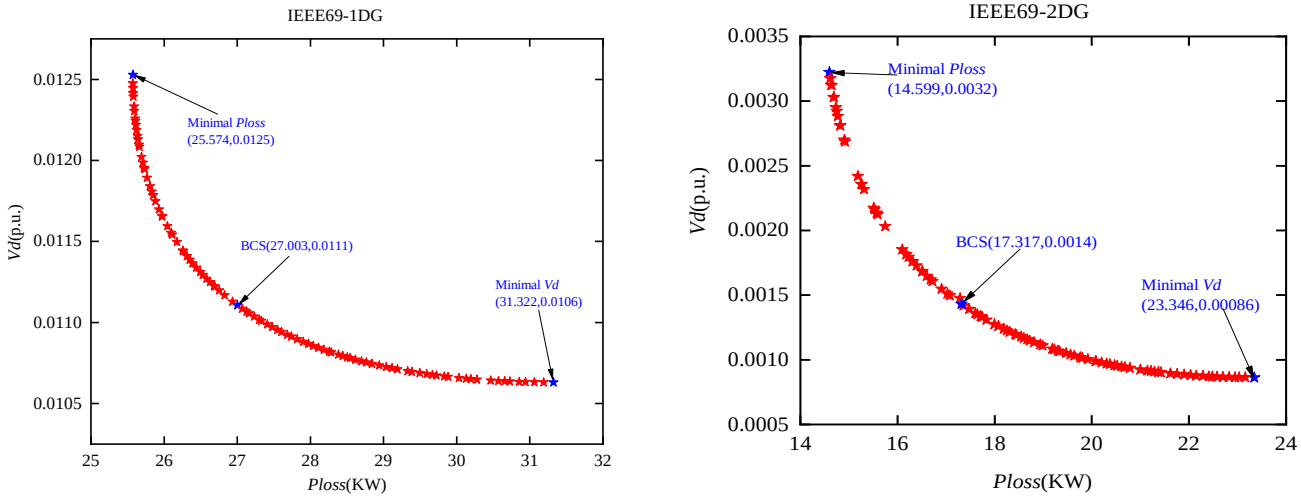

Fig. 26. PF curves in the IEEE-69 test system

V. Conclusion

In this paper, we examine the complex problem of combining the locations and capacities of DGs to minimise active loss and voltage deviation in radial distribution networks. This paper presents a sensitivity analysis technique and an enhanced ISC-SSA algorithm with a constraint strategy for single-objective problems. To increase the method's adaptability, the proposed sensitivity analysis method is combined with the Pareto non-inferiority ranking to develop the MOISC-SSA algorithm for multi-objective OADG problems. IEEE-33, IEEE-69, and IEEE-119 radial distribution networks are utilised to validate the efficacy and superiority of the method.

DGs providing both active and reactive power in reasonable configurations are more effective at reducing active power losses and improving voltage distribution than those providing only active power; Using the IEEE-33 node system as an example, the ISC-SSA algorithm reduces *Ploss* of the original system by 65.49 % in the configuration of 3DGs providing only active power. The original system's *Ploss* is reduced by 94.05% when 3DGs provide both active and reactive power. The results indicate that the ISC-SSA algorithm is more precise than the original SSA algorithm and other algorithms. In addition, the MOISC-SSA algorithm achieves uniformly distributed PFs in multi-objective experiments on two different-sized test systems, particularly when two DGs with a power factor of 0.8 are connected to the 69-node test system, while reducing *Ploss* and *Vd* by 92.30 and 98.59% more than the original system.

The ISC-SSA and MOISC-SSA algorithms based on constraint strategies proposed in this paper offer effective techniques for single- and multi-objective OADG problems, which are more advantageous for the economical and stable operation of radial distribution networks.

References

[1] M.P.H. A, P.D. Huy and V.K. Ramachandaramurthy, "A review of the optimal allocation of distributed generation: objectives, constraints, methods, and algorithms," *Renewable and Sustainable Energy Reviews*, vol. 75, pp. 293-312, 2017.

[2] P.A. Gkaidatzis, A.S. Bouhouras, D.I. Doukas, K.I. Sgouras and D.P. Labridis, "Load variations impact on optimal DG placement problem concerning energy loss reduction," *Electric Power Systems Research*, vol. 152, pp. 36-47, 2017.

[3] N. Khalesi, N. Rezaei and M.R. Haghifam, "DG allocation with application of dynamic programming for loss reduction and reliability improvement," *International Journal of Electrical Power & Energy Systems*, vol. 33, no. 2, pp. 288-295, 2011.

[4] P. Prakash and D.K. Khatod, "Optimal sizing and siting techniques for distributed generation in distribution systems: a review," *Renewable and Sustainable Energy Reviews*, vol. 57, pp. 111-130, 2016.

[5] P.S. Georgilakis and N.D. Hatziargyriou, "Optimal distributed generation placement in power distribution networks: models, methods, and future research," *IEEE Transactions on Power Systems*, vol. 28, no. 3, pp. 3420-3428, 2013.

[6] P.P. Biswas, R. Mallipeddi, P.N. Suganthan and G.A.J. Amaratunga, "A multiobjective approach for optimal placement and sizing of distributed generators and capacitors in distribution network," *Applied Soft Computing*, vol. 60, pp. 268-280, 2017.

[7] A.R. Jordehi, "Allocation of distributed generation units in electric power systems: a review," *Renewable and Sustainable Energy Reviews*, vol. 56, pp. 893-905, 2016.

[8] N.A. Khan, S. Ghosh and S.P. Ghoshal, "Optimal allocation and sizing of dg and shunt capacitors using differential evolutionary algorithm," *International Journal of Power and Energy Conversion*, vol. 4, no. 3, pp. 278-292, 2013.

[9] S.K. Sudabattula and K. M, "Optimal allocation of solar based distributed generators in distribution system using bat algorithm," *Perspectives in Science*, vol. 8, pp. 270-272, 2016.

[10] A. Fathy, D. Yousri, A.Y. Abdelaziz and H.S. Ramadan, "Robust approach based chimp optimization algorithm for minimizing power loss of electrical distribution networks via allocating distributed generators," *Sustainable Energy Technologies and Assessments*, vol. 47, article. 101359, 2021.

[11] N. Dharavat, S. Sudabattula and V. Suresh, "Optimal allocation of multiple distributed generators and shunt capacitors in a distribution system using political optimization algorithm," *International Journal of Renewable Energy Research-IJRER*, vol. 11, no. 4, pp. 1478-1488, 2021.

[12] S. Arulprakasam and S. Muthusamy, "Modified rainfall optimization based method for solving distributed generation placement and reconfiguration problems in distribution networks," *International Journal of Numerical Modelling: Electronic Networks, Devices and Fields*, vol. 35, no. 3, article. e2977, 2021.

[13] S. Sharma, K.R. Niazi, K. Verma and T. Rawat, "A bi-level optimization framework for investment planning of distributed generation resources in coordination with demand response," Energy Sources, Part A: Recovery, *Utilization, and Environmental Effects*, pp. 1-18, 2020.

[14] K. Ma, X. Liu, G. Li, S. Hu and J. Yang, "Resource allocation for smart grid communication based on a multi-swarm artificial bee colony algorithm with cooperative learning," *Engineering Applications of Artificial Intelligence*, vol. 81, pp. 29-36, 2019.

[15] G. Chen, A. Zhang, C. Zhao and Z. Zhang, "Optimal placement and capacity of combined DGs and SCs in radial distribution networks based on PSO-OS algorithm," *IAENG International Journal of Computer Science*, vol. 48, no. 2, pp. 236-249, 2021.

[16] G. Chen, X. Zhao, K. Peng, P. Zhou and X. Zeng, "Optimized configuration of location and size for DGs and SCs in radial distributed networks based on improved butterfly algorithm," *IAENG International Journal of Applied Mathematics*, vol. 52, no. 1, pp. 81-100, 2022.

[17] M.C.V. Suresh and J.B. Edward, "A hybrid algorithm based optimal placement of DG units for loss reduction in the distribution system," *Applied Soft Computing*, vol. 91, article. 106191, 2020.

[18] R. Rajaram, K.S. Kumar and N. Rajasekar, "Power system reconfiguration in a radial distribution network for reducing losses and to improve voltage profile using modified plant growth simulation algorithm with distributed generation (DG)," *Energy Reports*, vol. 1, pp. 116-122, 2015.

[19] A.M. Ibrahim and R.A. Swief, "Comparison of modern heuristic algorithms for loss reduction in power distribution network equipped with renewable energy resources," *Ain Shams Engineering Journal*, vol. 9, pp. 3347-3358, 2018.

[20] B. Das, V. Mukherjee and D. Das, "DG placement in radial distribution network by symbiotic organisms search algorithm for real power loss minimization," *Applied Soft Computing*, vol. 49, pp. 920-936, 2016.

[21] A. Noori, Y. Zhang, N. Nouri and M. Hajivand, "Multi-objective optimal placement and sizing of distribution static compensator in radial distribution networks with variable residential, commercial and industrial demands considering reliability," *IEEE Access*, vol. 9, pp. 46911-46926, 2021.

[22] A.M. Hemeida, O.M. Bakry, A.A. Mohamed and E.A. Mahmoud, "Genetic algorithms and satin bowerbird optimization for optimal allocation of distributed generators in radial system," *Applied Soft Computing*, vol. 111, article. 107727, 2021.

[23] M.H. Moradi, S.M.R. Tousi and M. Abedini, "Multi-objective PFDE algorithm for solving the optimal siting and sizing problem of multiple DG sources," *International Journal of Electrical Power & Energy Systems*, vol. 56, pp. 117-126, 2014.

[24] S. Nagaballi and V.S. Kale, "Pareto optimality and game theory approach for optimal deployment of DG in radial distribution system to improve techno-economic benefits," *Applied Soft Computing*, vol. 92, article. 106234, 2020.

[25] G. Chen, F.L. Lewis, E.N. Feng and Y. Song, "Distributed optimal active power control of multiple generation systems," *IEEE Transactions On Industrial Electronics*, vol. 62, no. 11, pp. 7079-7090, 2015.

[26] D.K. Khatod, V. Pant and J. Sharma, "Evolutionary programming based optimal placement of renewable distributed generators," *IEEE Transactions on Power Systems*, vol. 28, no. 2, pp. 683-695, 2013.

[27] S.G. Naik, D.K. Khatod and M.P. Sharma, "Optimal allocation of combined DG and capacitor for real power loss minimization in distribution networks," *International Journal of Electrical Power &*

Energy Systems, vol. 53, pp. 967-973, 2013.

[28] S. Mirjalili, A.H. Gandomi, S.Z. Mirjalili, S. Saremi and H. Faris, "Salp swarm algorithm: a bio-inspired optimizer for engineering design problems," *Advances in Engineering Software*, vol. 114, pp. 163-191, 2017.

[29] S. Mirjalili, "SCA: a sine cosine algorithm for solving optimization problems," *Knowledge-Based Systems*, vol. 96, pp. 120-133, 2016.

[30] I. Aljarah, M. Mafarja, A.A. Heidari, H. Faris and Y. Zhang, "Asynchronous accelerating multi-leader salp chains for feature selection," *Applied Soft Computing*, vol. 71, pp. 964-979, 2018.

[31] M.E. Baran and F.F. Wu, "Network reconfiguration in distribution systems for loss reduction and load balancing," *IEEE Transactions On Power Delivery*, vol. 4, no. 2, pp. 1401-1407, 1989.

[32] A. Selim, S. Kamel, A.S. Alghamdi and F. Jurado, "Optimal placement of DGs in distribution system using an improved harris hawks optimizer based on single- and multi-objective approaches," *IEEE Access*, vol. 8, pp. 52815-52829, 2020.

[33] T.P. Nguyen, T.A. Nguyen, T.V.H Phan and D.N. Vo "A comprehensive analysis for multi-objective distributed generations and capacitor banks placement in radial distribution networks using hybrid neural network algorithm," *Knowledge-Based Systems*, vol. 231, article. 107387, 2021.

[34] M.M. Aman, G.B. Jasmon, A.H.A. Bakar and H. Mokhlis, "Optimum network reconfiguration based on maximization of system loadability using continuation power flow theorem," *International Journal of Electrical Power & Energy Systems*, vol. 54, pp. 123-133, 2014.

[35] S. Kumar, K.K. Mandal and N. Chakraborty, "A novel opposition-based tuned-chaotic differential evolution technique for techno-economic analysis by optimal placement of distributed generation," *Engineering Optimization*, vol. 52, no. 2, pp.303-324, 2020.

[36] I.A. Quadri, S. Bhowmick and D. Joshi, "A comprehensive technique for optimal allocation of distributed energy resources in radial distribution systems," *Applied Energy*, vol. 211, pp. 1245-1260, 2018.

[37] T.P. Nguyen and D.N. Vo, "A novel stochastic fractal search algorithm for optimal allocation of distributed generators in radial distribution systems," *Applied Soft Computing*, vol. 70, pp. 773-796, 2018.

[38] S. Kumar, K.K. Mandal and N. Chakraborty, "Optimal DG placement by multi-objective opposition based chaotic differential evolution for techno-economic analysis," *Applied Soft Computing*, vol. 78, pp. 70-83, 2019.

[39] S. Sultana and P.K. Roy, "Multi-objective quasi-oppositional teaching learning based optimization for optimal location of distributed generator in radial distribution systems," *International Journal of Electrical Power & Energy Systems*, vol. 63, pp. 534-545, 2014.

[40] S. Sharma, S. Bhattacharjee and A. Bhattacharya, "Quasi-oppositional swine influenza model based optimization with quarantine for optimal allocation of DG in radial distribution network," *International Journal of Electrical Power & Energy Systems*, vol. 74, pp. 348-373, 2016.